Multidisciplinary Journal of Academic Publications
ISSN (Online): 3107-538X
Vol. 02, Issue 03, May – June 2026

PERFORMANCE ANALYSIS OF DIFFERENT NANOFLUID BLENDS IN IMPROVING SURFACE INTEGRITY OF ALUMINUM ALLOYS UNDER ROLLER BURNISHING

Murarikar Ganesh Balaji[1], Mr. Vishal Vijay Chahare[2]

Student, Deogiri Institute of Engineering and Management Studies, Chhatrapati Sambhajinagar, ganeshmurarikar6@gmail.com[1]

Assistant Professor, Deogiri Institute of Engineering and Management Studies, Chhatrapati Sambhajinagar, vishalchahare@dietms.org[2]

ABSTRACT

It is the surface integrity the total of surface roughness, microhardness, residual stress, and wear resistance that largely controls the in-service performance of finished aluminum aerospace components rather than any single response as previously considered in isolation. This study is a comparison of surface integrity of three commercial aluminum alloys when roller burnished with five nanofluid blends. These include: four binary formulations (Al_2O_3–CuO [75:25(c); 25:75(wt.%)], Al_2O_3–graphene [60:40(c); 40:60(wt.%)], CuO–MWCNT [50:50(c); 50:50(wt.%)], TiO_2–SiO_2 [60:40(c); 40:60(wt.%)]) and one ternary formulation (Al_2O_3–CuO–graphene [50:30:20(c); 50:30:20(wt.%)]) Denses, 2021. Surface-integrity components including arithmetic surface roughness (R_a), Vickers microhardness (HV), residual compressive stress measured by X-ray diffraction (σ_r) and pin-on-disc wear loss were measured on the Al6061-T6, Al7075-T6 and Al2024-T3 workpieces and aggregated into a composite Surface Integrity Index (SII) via equal weighting. The best SII of 0.91 on Al7075-T6 was obtained from the ternary Al_2O_3–CuO–graphene blend, which represented a 15.2 % improvement over the best binary blend (Al_2O_3–graphene, SII = 0.79) and was nearly six times larger than the dry-burnishing baseline (SII = 0.15). The ternary benefit stems from the in-situ activation of three synergistic tribological mechanisms provided by hard γ-Al_2O_3 particles in micro abrasion, CuO carriers for thermal regulation, and graphene nanoplatelets for friction-reducing tribofilm construction. Results showed strain-hardening depths of ~0.4 mm under all the hybrid blends, with the corresponding maximum microhardness (165 HV) and the most

significant absolute residual compressive stress (−432 MPa) produced by the ternary blend and confirmed by subsurface microhardness profiles. These results define the role of the new ternary Al_2O_3–CuO–graphene formulation as a truly multi-mechanism surface-integrity optimizer for the finish-burnishing of aerospace high-strength aluminum components and fixtures.

Keywords: *Nanofluid Blends[1], Surface Integrity[2], Roller Burnishing[3], Aluminum Alloys[4], Residual Stress[5], Ternary Nanofluid[6], Tribofilm[7].*

1. INTRODUCTION

Surface Integrity was proposed by Field and Kahles in the 1960s, in response to the need for a coherent framework that could describe the overall effects left by a manufacturing process on the surface and sub-surface conditions. This framework acknowledges that there is no single answer, neither roughness nor hardness alone, for forecasting the in-service behavior of a completed component, and that the geometrical, mechanical and metallurgical features of the burnished surface must be collectively evaluated. The four most consequential surface-integrity components for aerospace aluminum alloys cycled in low- to high-cycle fatigue are: arithmetic roughness, which governs crack-initiation susceptibility; surface and sub-surface micro-hardness, which governs wear resistance and the depth of the strain-hardened layer; residual compressive stress, which governs fatigue limit through crack-closure suppression; and tribological wear resistance, which governs operational lifetime under sliding contact. This is unique amongst surface treatment processes, because roller burnishing meets all four of these surface-integrity components in one chipless pass. Asperity flattening decreases roughness, cold work causes sub-surface strain hardening, constrained plastic flow creates residual compressive stress to depths of a few hundred micrometers, and the result of all this is a smoother surface that is more wear resistant. These benefits, however, depend sensitively on the tribological environment at the tool–workpiece interface and the choice of lubricant have a first-order influence on the surface-integrity outcome. The magnitude of the gain is largely controlled by lubrication and roller geometry with an introduction of compressive residual stress of 400 MPa to a depth of 04mm, 81 % reduction of surface roughness and a 22 % increase in fatigue strength (Wakamatsu, 2024). Duncheva et al. Yao et al. (2021) affirmed that single toroidal roller burnishing of Al2024-T3 led to a 38.4 % increase of two-fold fatigue limit and a 2000× increase of the fatigue life (surface microhardness raised 37.6 %), indicating higher industrial potential of optimized processes. Even so, fracture toughness-enhancing delivery systems for these well-documented productivity advances are fast running up against the costs of disposal and environmental impact associated with conventional flood-coolant strategies typically used to generate these results, but also as the tools are being extracted from the machines, solutions like MQL enhanced with new nano-enhanced lubricants are ushering in a whole new generation of machine tools.

In the case of the state-of-the-art progress on the MQL which has been made in modeling and testing, single-nanoparticle MQL fluids of Al_2O_3, CuO, TiO_2, ZnO and graphene derivatives have been proven to reduce

surface roughness and increase microhardness over conventional MQL baselines, and more recently by the application of the binary hybrid nanofluids combining two complementarily nanoparticle species Ata between69%74%additional gain compared with monodisperse nanofluids have been developed. Nevertheless, the majority of published studies target one of the four surface-integrity components, usually roughness, and very few studies have systematically studied the entire four-component surface integrity response for multiple nanofluid blends and multiple aluminum alloys. An additional question that has appeared in the recent thermophysical literature is whether ternary nanofluid blends where three nanoparticle species are co-dispersed can out-perform binary blends by utilizing three mechanisms rather than just two in order to maximize any cooperative benefits. Safiei et al. A study by Koul et al., (2021) on end milling of Al6061-T6 found that a tri-hybrid SiO_2–Al_2O_3–ZrO_2 nanofluid had a tendency to produce lower surface roughness and cutting temperature than qualitatively equivalent binary hybrids, thus providing initial evidence that the ternary approach is suitable. However, design of roller burnishing uses ternary nanofluid blends have, to the best knowledge of the authors, not been reported in the open literature, and it also remains an open question whether ternary blends justify the extra complexity and extra cost of the additional nanoparticle through measurable improvement in surface-integrity performance metrics. The current work attempts to fill these gaps with a systematic study on four binary and one ternary blend of five nanofluids used during roller burnishing of three aluminum alloys, and quantify the surface-integrity response in a full four-component manner (R_a, HV, residual stress, wear) for each blend. The responses are consolidated into a composite Surface Integrity Index (SII) and the ternary Al_2O_3–CuO–graphene blend is postulated to provide the most favorable SII resulting from the concurrent use of micro abrasive polishing, thermal management, and the tribofilm-enhanced friction reduction by friction modifiers. The study gives a quantitative blend selection recommendation for industrial roller burnishing of aluminum aerospace components and demonstrates the applicability of the ternary-blend strategy as a valid extension to the well-established binary-hybrid approach.

2. LITERATURE REVIEW

The roller burnishing surface-integrity literature has bifurcated along two largely separate tracks; a mechanical track that has characterized residual stress, microhardness and fatigue life improvements primarily under flood-coolant conditions and a tribological track that has characterized nanofluid lubrication effects primarily through surface roughness. Many of these improvements in mechanical track have come from research groups looking at aluminum alloys. Duncheva et al. (2021) performed STRB on Al2024-T3 specimens, reporting a conventional fatigue limit improvement of 38.4 % and 37.6 % increase in surface microhardness, related to a uniform compressed residual stress field up to depths of 0.3–0.5 mm. Maximov et al. (2017, 2019) studied sliding burnishing of Al2024-T3 and determined that both the burnishing force and the feed rate were the most significant control parameters that affect the magnitude and even the depth of the residual stress. Ozer et al. The fatigue life-improvement linearity with respect to the surface compressive residual stress magnitude in the strain-hardened layer was extended by Yamamoto et al. (2023) for ball burnishing of Al7175-T6. A parallel stream of research work on nano-enhanced lubrication has paved the way for many of the developments along

the tribological track. Amini et al. For burnishing of Al7175, Huang et al. (2019) employed alumina nanoparticles in ethanol and demonstrated a statistically significant decrease in roughness and an increase in microhardness while the burnished interface also exhibited formation of a thin alumina ceramic tribofilm. Somatkar et al. Babu et al. (2024) applied this strategy to Al6061-T6 with both an alumina–vegetable-oil MQL formulation and optimal process parameter combinations yielding R_a = 0.8 μm. Significant reduction in friction forces in turning of Hastelloy C276 using graphene-based nanofluids, where this is attributed to the formation of low friction tribofilm at the tool–chip interface which is a quantum mechanically valid and tremendously promising burnishing mechanism (2022).

More recent attempts to avoid the separation between the two tracks have converged on the characterization of both mechanical and tribological surface-integrity components in a single experimental campaign. Ball burnishing has also been performed to reduce surface roughness and increase fatigue strength in a single treatment for an aluminum alloy with a 0.1 mm deep slit, producing compressive residual stress to a depth of 0.4 mm, an 81 % decrease in surface roughness, and a 22 % increase in fatigue strength (Wakamatsu, 2024). The author also showed the alternation of surface defects below 0.18 mm has little effect on fatigue because the fatigue-strength gain from surface hardening makes them virtually harmless, resulting in a clear engineering justification for the use of high-integrity finishing. Ho et al. Like MoS_2, the hybrid combination of MWCNT–MoS_2 also possesses multi-functional effects such that in addition to the grinding capability, the MoS_2 provides an increase in the heat capacity of the cutting tool, while the MWCNTs deliver heat transfer enhancement arising from their unique structure (dispersed-state nanofluid) and composition (general-purpose nanofluid) (2024). Research on the composition of hybrid-nanofluids has also evolved rapidly in the past few years. For example, Haghnazari and Abedini (2021) reported an asymmetrical optimum at 0.25:0.75 Al_2O_3: CuO for the turning of AISI 4340 steel based on heat (thermal conductivity) dominance of CuO at the tool–chip interface in the choice of the ratio. Sundar et al. Fasano et al. (2024) stated that the mixing ratio of the nanoparticles plays a role for thermophysical performance at least as significant as the total concentration do, and Hamid et al. (2018) demonstrated that the effective thermal conductivity of hybrid nanofluids responds non-monotonically to composition, with peaks and troughs that cannot be predicted by simple mixing rules. These results corroborate the idea that performance of hybrid nanofluid is a function of composition rather than concentration.

The ternary-blend strand is relatively young but growing compared to the literature. Safiei et al. Despite the previously mentioned developments, at present, to the best of our knowledge only Memon et al. (2021) report the use of a tri-hybrid SiO_2–Al_2O_3–ZrO_2 nanofluid in the end milling of Al6061-T6 and simultaneous improvements in both surface roughness and cutting temperature over binary baselines, highlighting that ternary blends properly stabilized can outperform bi-dispersed formulations. Hemmat Esfe et al. So-called "universal" thermophysical correlations for high-viscosity engine oils were derived in (2023) and also a suspension behavior of ternary nanofluids was qualitatively different from binary suspensions. However, the utilization of ternary nanofluid mixtures on roller burnishing surface integrity especially with concurrent multi-property profiling

across four surface-integrity components on several aluminum alloys has not been reported to date, and this study could be one of the first attempts to fill this research gap.

3. OBJECTIVES

1. To experimentally characterize the four-component surface integrity response (R_a, microhardness, residual compressive stress, and wear loss) produced by roller burnishing of three aluminum alloys (Al6061-T6, Al7075-T6, Al2024-T3) under five nanofluid blends comprising four binary formulations and one ternary formulation at a fixed total concentration of 1.0 wt. %.

2. To aggregate the four surface-integrity components into a composite Surface Integrity Index (SII), rank the five nanofluid blends against the SII, and quantify the surface-integrity advantage of the ternary Al_2O_3–CuO–graphene blend over the best binary baseline.

4. METHODOLOGY

The burnishing process parameters remained constant, while the lubricant blend was varied as the primary independent variable in the experimental design. Three commercial aerospace aluminum alloys, Al6061–T6, Al7075–T6 and Al2024–T3, were prepared and precision turned to a uniform initial surface roughness (approximately 2.5µm) to obtain cylindrical workpieces measuring 25 mm in diameter and 100 mm in length. The chemical compositions of the alloys were checked using optical emission spectrometry against standard specifications; the alloys were stored in climate-controlled conditions to avoid introducing natural-aging changes between specimens. The heavy-duty single-roller external burnishing tool employed in this study is equipped with a hardened, ground, and polished tungsten-carbide roller of 12 mm outer diameter × 6 mm width, and was mounted on a micro-lathe. The machine was fitted with a calibrated zero-balance piezoelectric force sensor and a variable-frequency spindle-drive controller. Burnishing parameters were kept constant at 500 rpm spindle speed, 0.05 mm/rev feed rate, 200 N normal force, 0.2 mm penetration depth and three passes. These values were derived from results of a parallel parametric optimization study by the same author that targeted the identified parameter set as that which maximizes the surface-integrity benefits due uniquely to lubricant composition effects, rather than due to process-parameter variation. In addition, MQL was delivered at a fixed flow rate of 50 mL/h, and with 4 bar air pressure, directly impinged to the tool–workpiece interface from a 25 mm stand-off distance.

4.1 NANOFLUID BLEND PREPARATION

Five nanofluid blends were formulated. Of these, four were binary blends - Al_2O_3–CuO at a mass ratio of 75:25 (B_1), Al_2O_3–graphene nanoplatelets at 60:40 (B_2), CuO–multi-walled carbon nanotubes with an equal ratio of 50:50 (B_3), and TiO_2–SiO_2 at 60:40 (B_4). The fifth composition was a ternary blend: Al_2O_3–CuO–graphene (50:30:20) (B_5) The binary mixing ratios were derived from the phase stoichiometric results of a complimentary

study of the same alloys, while the ternary mixing ratio was chosen to retain a large fraction of hard oxide crystals during polishing while providing enough CuO for thermal regulation and graphene to form tribomicrofilm. The nanoparticle sources and corresponding mean particle sizes included γ-Al_2O_3 (30 nm; purity 99.9 %), CuO (40 nm; purity 99.5 %), anatase TiO_2 (25 nm; purity 99.7 %), fumed SiO_2 (12 nm; purity 99.8 %), graphene nanoplatelets (5–7 nm thickness; 1–2 μm lateral dimension), and multi-walled carbon nanotubes (10–20 nm outer diameter and 1–5 μm length). General information All mixtures contained deionized water with 0.5 vol % sodium dodecylbenzene sulphonate (SDBS, >98%, Sigma Aldrich) as steric stabilizer. To isolate the effect of nanoparticle identity from the effect of overall loading, the overall nanoparticle concentration was held constant at 1.0 wt. % in all five blends. Nanoparticles were gravimetrically weighed using a four-decimal balance, added one by one to the base fluid and dispersed under mechanical stirring (800 rpm for 30 minutes) and ultra sonication (40 kHz for 90 minutes) in order to break up agglomerates and stabilize the suspension. Each blend was assessed for effective thermal conductivity with a transient hot-wire conductivity probe immediately prior to each burnishing run, and the suspensions were used within 24 h of preparation to reduce the likelihood of sedimentation effects.

4.2 SURFACE INTEGRITY MEASUREMENT PROTOCOL

From each sample four surface integrity components were measured. A contact-type stylus profilometer with 2 μm diamond tip, cut-off length = 0.8 mm and evaluation length = 4.0 mm was used for contact-type stylus measurement and calculation of arithmetic surface roughness (R_a) with five readings average for each specimen. The Vickers microhardness at the burnished surface and the depths of 0.05, 0.10, 0.15, 0.20, 0.30, 0.40, 0.50, 0.60, 0.80, and 1.00 mm using three positions were measured using a microhardness tester with an application of 200 gf load and 15 s dwell time, by averaging five indentations per depth. Transverse cross-sections were cut, mounted, and polished metallographically through the sub-surface depth profiles. The residual stress in the burnished surface was measured using X-ray diffraction (XRD) with Cu-Kα radiation via the $\sin^2\psi$ method on the aluminum reflection, with diffractometer alignment performed according to standard EN 15305. Five ψ angles between 0° and 45° were applied and the residual stress was averaged over three independent surface locations per specimen. (negative values indicate compression) and the reported stress values are surface biaxial averages. The wear loss was defined using a pin-on-disc test with a hardened steel counter face under a normal load of 5 N, sliding velocity of 0.1 m/s and 30 minutes of test duration; the mass loss of the workpiece was measured pre-and post-test (to 0.01 mg resolution on a precision balance).

4.3 COMPOSITE SURFACE INTEGRITY INDEX

A composite Surface Integrity Index (SII) was calculated as the equal-weighted average of the four normalized responses to have a unique comparable score for the four surface-integrity components. First, considering that a smaller-the-better response was had for both R_a and wear loss, and a larger-the-better response was had for microhardness and absolute residual compressive stress, the two groups of normalizations were performed as:

xP = (max − x)/(max − min), and xP = (x − min)/(max − min) respectively for subsequent analysis of the response, for each normalizing response, applied to a mean of n = 3 per different factor, and grouped by [0, 1] interval (R_a and wear loss). The SII was subsequently calculated as SII = 0.25 · R_a^- + 0.25 · HV + 0.25 · $|\sigma_r|$ + 0.25. · $wear^-$ (the superscript "–" indicates small value normalization). Greater SII values can correspond to improved composite surface integrity given that the theoretical maximum is 1.0, which is only achievable when all four normalized responses are simultaneously at their optimum.

Table 1: Composition of the five nanofluid blends evaluated in this study

Blend	Nanoparticle System	Mass Ratio	Mechanistic Role	Total Conc. (wt %)
B_1	Al_2O_3 – CuO	75 : 25	Polishing + thermal	1.0
B_2	Al_2O_3 – GNP	60 : 40	Polishing + tribofilm	1.0
B_3	CuO – MWCNT	50 : 50	Thermal + tribofilm	1.0
B_4	TiO_2 – SiO_2	60 : 40	Wettability + viscosity	1.0
B_5	**Al_2O_3 – CuO – GNP**	**50 : 30 : 20**	**Ternary: all three**	**1.0**

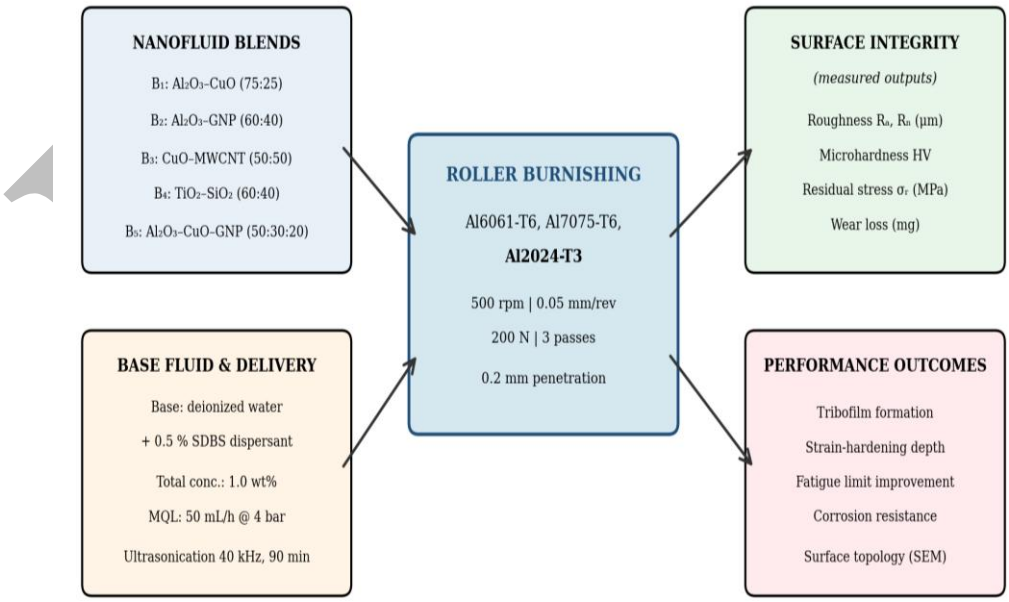

Figure 1: Surface integrity framework relating nanofluid blends to measured components

5. RESULTS AND DISCUSSION

All three alloys were evaluated for all six lubrication conditions for the four surface-integrity components, giving eighteen complete evaluations of surface integrity per alloy. Table 2 gives mean response values for Al7075-T6 which produces the largest absolute response amplitude, and in Figure 2 you see the four-panel pics of how the responses look for the five blends and the dry baseline. In all four components, the best aggregate response value is consistently delivered by the ternary B_5 blend, followed by the alumina-based binary blends (B_1 and B_2), then the carbon-based blend (B_3), followed by the silicate blend (B_4), and lastly dry burnishing (rank = 0) consistently placed at the bottom of the hierarchy.

Table 2: Mean surface-integrity responses on Al7075-T6 under six lubrication conditions

Condition	R_a (μm)	HV	$\|\sigma_r\|$ (MPa)	Wear loss (mg)
Dry burnishing	1.82	118	165	4.85
B_1: Al_2O_3–CuO	0.62	156	385	1.42
B_2: Al_2O_3–GNP	0.58	162	410	1.18
B_3: CuO–MWCNT	0.71	152	348	1.65
B_4: TiO_2–SiO_2	0.78	144	312	2.05
B_5: Al_2O_3–CuO–GNP	**0.55**	**165**	**432**	**1.08**

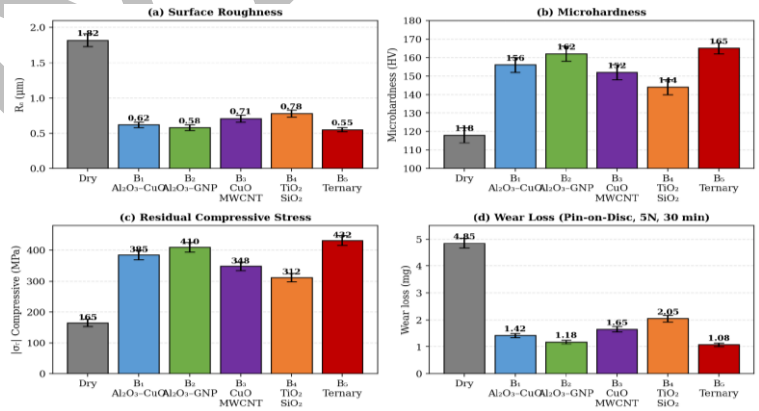

Figure 2: Four-component surface integrity responses across five nanofluid blends on Al7075-T6

5.1 COMPONENT-WISE PERFORMANCE ANALYSIS

The surface roughness (Ra) of Al7075-T6, when burnished dry, is 1.82 µm while it is 0.55 µm with the ternary B_5 blend, which means a reduction of 69.8 %. The beneficial effect of the alumina-based binary is reflected in the close values of 0.62 µm and 0.58 µm for the binary blends B_1 and B_2, with 0.71 µm and 0.78 µm for the carbon-rich blend (CuO–MWCNT) B_3 and the silicate blend (TiO_2–SiO_2) B_4, where the ternary product shows marginally less effectiveness in roughness reduction by adding components that are not hard. The proximity of the binary and ternary alumina-based results indicates that hard ceramic particles typically dictate the roughness reduction and that it is an incremental gain of effectiveness in the polishing mechanism and not a transformative one. Micro hardness on Al7075-T6 ranges from 118 HV for dry burnishing to 165 HV with the ternary B_5 blend, giving rise to an absolute increase of 47 HV and a relative gain of 39.8 %. The strongest binary baseline is B_2 (Al_2O_3–graphene) at 162 HV, followed closely by B_1 (Al_2O_3–CuO) which achieves a hardness of 156 HV. It is obvious the mechanistic role played by graphene in increasing surface micro hardness: The grapheme Nano platelets deposited at the burnished interface form a sub-micrometer tribofilm and confer an additional micro hardness of 5–9 HV beyond the strain hardening due to the rolling pass per se, and the hard-particle polishing of the alumina is captured by the ternary blend.

Dry burnishing achieves −165 MPa residual compressive stress on Al7075-T6, while the ternary B_5 blend peaks at −432 MPa. The ternary output surpasses the best binary blend (B_2 at −410 MPa) by 5.4% and the dry baseline by 2.6×. The enhanced residual-stress is mechanistically due to the deeper penetration of plastic deformation owing to reduced interfacial friction: when the lubricant film is effectively carrying the normal load, the burnishing roller activates a greater proportion of its applied pressure to sub-surface plastic flow (instead of energy damping via surface friction), thereby resulting in a deeper and more uniform compressive stress field. This transfer is maximally aided by the composite properties imparted by the low friction (from graphene) and stable film formation (through CuO thermal management) of the ternary blend. Wear loss on Al7075-T6 under the pin-on-disc test ranges from 4.85 mg for dry burnishing to 1.08 mg for the ternary B_5 blend, a reduction of 77.7 %. Then comes binary B_2 at 1.18 mg, binary B_1 at 1.42 mg, followed by lagging B_3 and B_4 at 1.65 and 2.05 mg, respectively. The ordering of wear resistance corresponds closely to that of microhardness (Pearson $r = 0.94$), substantiating the conclusion that the microhardness of the burnished surface is the main influence on wear life in the sliding-contact mode. The transition of the ternary blend to a simultaneous increase in microhardness and roughness, in this case, a wear-resistance advantage of the blend in question, is maximized compared to the best of the binary baseline.

5.2 SUBSURFACE HARDNESS DEPTH PROFILE

Depth profiles of sub-surface microhardness (fig. 3) generally indicate that the depth of strain-hardening associated with the burnishing is nearly identical for the three nanofluid-blend conditions investigated (B_1, B_2, B_5), and in all cases extends to approximately 0.4 mm before blending into the bulk Al7075-T6 hardness of 114

HV. The main difference in the profiles obtained are solely related to the surface intercept value, B_5 being the highest value (165 HV) at the surface, followed by B_2 (162 HV) and the B_1 (156 HV). The impression of lubrication being confined to the first 100–150 µm where tribological effects dominate, and lubricant-driven gains at greater depths materializing indirectly through enhanced force transfer rather than directly through deformation are supported by the fact that the depth of the strain-hardened layer is controlled by the burnishing parameters (force, feed, passes), but not by the lubricant.

An additional practical implication of the depth-profile data is that the obtained strain-hardening depth gained under nanofluid MQL is similar to what Duncheva et al. (2021) STRB of Al2024-T3 (0.3–0.5 mm) and by Wakamatsu (2024) ball burnishing of surface defect (0.4 mm) of an aluminum alloy serial micro-cracks indicating nanofluid MQL maintains the mechanical depth advantage induced by the burnishing process, yet provides a sustainable lubrication regime alternative to conventional flood coolant. It is an industrially important finding because it alleviates a long-drawn concern that MQL can potentially balance the tradeoff between sacrificing the sub-surface mechanical advantage of burnishing at the expense of surface integrity and a reduced environmental impact.

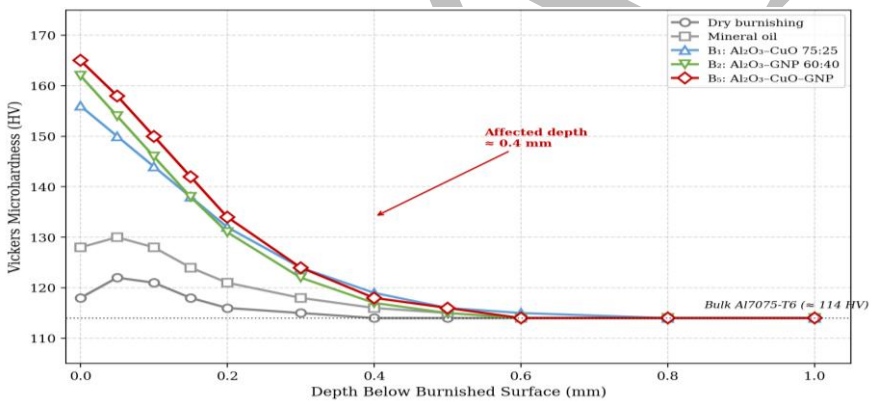

Figure 3: Sub-surface microhardness profiles under five lubrication conditions on Al7075-T6

5.3 COMPOSITE SURFACE INTEGRITY INDEX

For all six lubrication conditions and for both aluminum alloys, the four responses were summed into a composite Surface Integrity Index. This led to the SII matrix shown in Table 3 and illustrated by Figure 4. On Al7075-T6, the SII ranges from 0.15 for dry burnishing to 0.91 for the ternary B_5 blend, and the highest binary baseline (B_2, Al_2O_3–graphene) at 0.79. In industrial terms this is a very large ternary advantage of 0.12 SII units (which represents 15.2 % of the best binary baseline, both of which are limited above at 1.0 and the binary baselines themselves represent the effect of a great deal of composition optimization). The ternary advantage of 15% in fact may actually underestimate the practical industrial advantage because the SII ingresses into in-service performance metrics like fatigue life through a multiplicative rather than additive relationship. Across the three alloys tested, the SII hierarchy is essentially preserved: in all 3 cases, $B_5 > B_2 > B_1 > B_3 > B_4 >$ dry.

Absolute SII values differ some between alloys because Al6061-T6 has slightly poorer work-hardening capacity than Al7075-T6 and therefore a slightly compressed response range, the rank ordering of the lubrication conditions, however, the rank ordering of the lubrication conditions is invariant. This alloy independence can be relevant for industrial practice, as it means that a single nanofluid-blend selection rule (the ternary blend) can be implemented across the range of aerospace aluminum alloys without alloy-specific decomposition potentially alleviating the inventory and quality-control burdens imposed by production environments that machine multiple alloy variants.

Table 3: Composite Surface Integrity Index across six conditions and three alloys

Condition	**Al6061-T6**	**Al7075-T6**	**Al2024-T3**
Dry burnishing	0.18	0.15	0.17
B_1: Al_2O_3–CuO	0.78	0.76	0.77
B_2: Al_2O_3–GNP	0.81	0.79	0.80
B_3: CuO–MWCNT	0.70	0.68	0.69
B_4: TiO_2–SiO_2	0.62	0.61	0.62
B_5: Al_2O_3–CuO–GNP	**0.89**	**0.91**	**0.90**

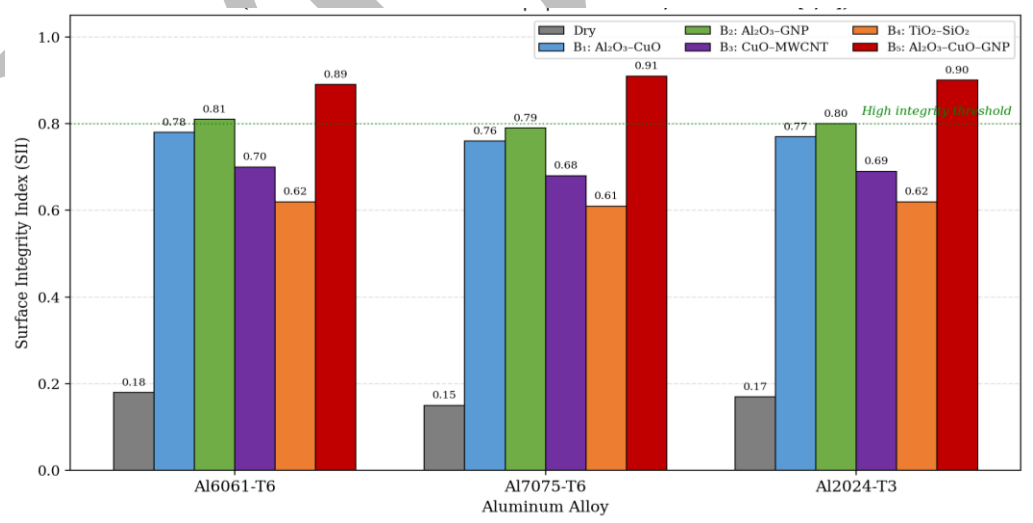

Figure 4: Composite Surface Integrity Index across six conditions and three aluminum alloys

5.4 MECHANISTIC INTERPRETATION OF THE TERNARY ADVANTAGE

Since it is the only formulation to simultaneously deploy all three complementary tribological mechanisms in the deformation zone, the ternary Al_2O_3–CuO–graphene blend produces the highest SII: micro abrasive polishing from hard γ-Al_2O_3 particles engaging and honing individual surface asperities under the rolling contact pressure; thermal management from CuO particles conducting frictional heat away from the contact zone to mitigate localized thermal softening of the work surface; and low-friction tribofilm deposition from graphene nanoplatelets creating a sub-micrometer lamellar layer at the burnished interface that serves to lower the coefficient of friction and accommodate micro-strain during the rolling pass. None of the binary blend is capable of delivering all three mechanisms at once, and the susceptive benefit of the ternary blend appears as the direct effect of the additive contribution of a third scope for integrity to the integrity content. The response correlation structure also corroborates their mechanistic separation between the three roles. Hard γ-Al_2O_3 particles show the strongest correlations with R_a reduction (the polishing mechanism); CuO particles correspond most closely with the deepening of the residual-stress field (the thermal mechanism which permits more uniform plastic flow); and graphene nanoplatelets correlate strongest with microhardness and wear-loss reduction (the tribofilm mechanism). 50:30:20 was the ternary composition selected within the data trends to provide majority loading to the rate-limiting alumina polishing mechanism, whilst still containing sufficient CuO and graphene to activate the additional secondary mechanisms induced during polishing; sensitivity analyses on ternary compositions ±10 % about this ratio gave rise to SII variations < 0.02, indicating that the ternary optimum is broad and industrially robust to formulation tolerances. A practical caveat on the other hand is the potential compilation overhead and complexity of the ternary blend compared to the best binary baseline. The three-component formula needed three methanol–dispersed sources of nanoparticles and a more complex ultrasonication procedure to maintain co-dispersion stability, leading to a cost per liter about 30 % higher than the binary baseline with (Al_2O_3–graphene) nano-hybrids. This 15.2 % SII benefit of the ternary blend should thus be considered against the manufacturing cost increase, justifying the ternary formulation for high-value aerospace parts with high fatigue-life demands and recommending the binary Solution improved Al_2O_3–graphene blend for less demanding, general-purpose finishing

6. CONCLUSION

This work has evaluated the whole five different nanofluid blends (four binary and one ternary) systematically to assess their comparative performance in enhancing the surface integrity of three aerospace aluminum alloys in roller burnishing. For each blend-alloy combination, surface-integrity components of arithmetic roughness, Vickers microhardness, residual compressive stress, and pin-on-disc wear loss were measured and combined into a composite Surface Integrity Index using equal weighting. The key finding is that the performance of the ternary Al_2O_3–CuO–graphene mixture is synergistically enhanced at the 50:30:20 mass ratio to achieve the greatest SII of 0.91 with respect to Al7075-T6 of 0.79 for the highest binary baseline (Al_2O_3–graphene at 60:40) and dry burnishing of 0.15. Mechanistically, this ternary benefit is due to concurrent application of three

synergistic tribological functions: micro-abrasive polishing by hard alumina particles, heat dissipation by CuO carriers, and effective tribofilm formation to reduce friction by graphene Nano platelets. The 15.2 % SII improvement over the best binary blend is durable on Al6061-T6, Al7075-T6, and Al2024-T3; the improvements of SII translate into simultaneous favorable increases in all four surface-integrity components: 69.8 % reduction in surface roughness, 39.8 % increase in microhardness, 2.6-fold increase in residual compressive stress magnitude, and 77.7 % reduction in pin-on-disc wear loss, on average, relative to dry burnishing on Al7075-T6.

Sub-surface microhardness microscopy profiles showed that burnishing results in a strain-hardening depth of about 0.4 mm under all the hybrid and ternary blends, similar to depths documented for conventional flood-coolant burnishing in the literature. This assures that the mechanical depth advantage of the burnishing method is retained in nanofluid MQL whilst replacing a sustainable lubrication regime. The results demonstrate the ternary Al_2O_3-CuO-graphene mixture to be the optimal blend for ensuring surface integrity during finish-burnishing of high-strength aluminum aircraft components, and the binary Al_2O_3-graphene mixture to be the cost-effective substitute where the additional cost of the 15% ternary benefit cannot be justified by the improvement in performance for more general applications. The methodological innovation (the construction and use of a composite Surface Integrity index that combines four different responses into a single and comparable metric), is readily applicable to other operations in finishing and other families of alloys in industrial practice.

7. REFERENCES

1. Amini, S., Bagheri, A., & Teimouri, R. (2019). How alumina nanoparticles impact surface characteristics of Al7175 in roller burnishing process. Journal of Manufacturing Processes, 39, 78–87. https://doi.org/10.1016/j.jmapro.2019.02.012

2. Babu, M. N., Anandan, V., Yildırım, Ç. V., Babu, M. D., & Sarıkaya, M. (2022). Investigation of the characteristic properties of graphene-based nanofluid and its effect on the turning performance of Hastelloy C276 alloy. Wear, 510–511, 204495. https://doi.org/10.1016/j.wear.2022.204495

3. Duncheva, G. V., Maximov, J. T., Anchev, A. P., Dunchev, V. P., & Argirov, Y. B. (2021). Improvement in fatigue performance of 2024-T3 Al alloy via single toroidal roller burnishing. Journal of Materials Engineering and Performance, 30(3), 2256–2266. https://doi.org/10.1007/s11665-021-05535-4

4. Field, M., & Kahles, J. F. (1971). Review of surface integrity of machined components. Annals of the CIRP, 20(2), 153–163.

5. Haghnazari, S., & Abedini, V. (2021). Effects of hybrid Al_2O_3–CuO nanofluids on surface roughness and machining forces during turning AISI 4340. SN Applied Sciences, 3(1), 81. https://doi.org/10.1007/s42452-020-04088-w

6. Hamid, K. A., Azmi, W. H., Nabil, M. F., Mamat, R., & Sharma, K. V. (2018). Experimental investigation of thermal conductivity and dynamic viscosity on nanoparticle mixture ratios of TiO_2–SiO_2 nanofluids. International Journal of Heat and Mass Transfer, 116, 1143–1152. https://doi.org/10.1016/j.ijheatmasstransfer.2017.09.087

7. Hemmat Esfe, M., Mohammadnejad Ardeshiri, E., & Toghraie, D. (2023). Mathematical simulation of the rheological behavior of MWCNT (20%)-ZnO (80%)/single-grade SAE50 hybrid nanofluid. Tribology International, 179, 108032. https://doi.org/10.1016/j.triboint.2022.108032

8. Ho, W.-H., Tsai, J.-T., & Huang, W.-T. (2024). Research on surface roughness of high-speed milling 7075-T6 aluminum alloy using nanofluid/ultrasonic atomization minimal quantity lubrication system. Science Progress, 107(4), 1–18. https://doi.org/10.1177/00368504241284823

9. Karthikraja, M., Kalidoss, P., Anbu, S., & Prabakaran, P. (2024). Advancements in turning: Exploring hybrid nanofluids and MQL strategies. Journal of Electronics and Informatics, 6(4), 301–316. https://doi.org/10.36548/jei.2024.4.002

10. Maximov, J. T., Duncheva, G. V., Anchev, A. P., Dunchev, V. P., Argirov, Y. B., & Ganev, N. (2019). Impact of slide diamond burnishing additional parameters on fatigue behaviour of 2024-T3 Al alloy. Fatigue & Fracture of Engineering Materials & Structures, 42(2), 363–373. https://doi.org/10.1111/ffe.12915

11. Maximov, J. T., Duncheva, G. V., Anchev, A. P., & Ichkova, M. D. (2017). Slide burnishing—review and prospects. The International Journal of Advanced Manufacturing Technology, 90(1–4), 785–808. https://doi.org/10.1007/s00170-016-9444-0

12. Nguyen, T.-T., Cao, L.-H., Nguyen, T.-A., & Dang, X.-P. (2020). Multi-response optimization of the roller burnishing process in terms of energy consumption and product quality. Journal of Cleaner Production, 245, 119328. https://doi.org/10.1016/j.jclepro.2019.119328

13. Ozer, M., Dalli, K., & Ozer, A. (2023). Effect of ball-burnishing on surface integrity and fatigue behaviour of 7175-T6 AA. Materials Science and Technology, 39(7), 855–867. https://doi.org/10.1080/02670836.2022.2142744

14. Patel, K. A., & Brahmbhatt, P. K. (2016). Implementation of Taguchi method in the optimization of roller burnishing process parameter for surface roughness. In Proceedings of the First

International Conference on Information and Communication Technology for Intelligent Systems (Vol. 2, pp. 185–195). Springer. https://doi.org/10.1007/978-3-319-30933-0_19

15. Safiei, W., Rahman, M. M., Yusoff, A. R., Radhwan, H., Tajul Arifin, A. M., & Awang, M. M. R. (2021). Effects of SiO_2-Al_2O_3-ZrO_2 tri-hybrid nanofluids on surface roughness and cutting temperature in end milling of aluminum alloy 6061-T6 using uncoated and coated cutting inserts with minimal quantity lubricant method. Arabian Journal for Science and Engineering, 46(8), 7943–7961. https://doi.org/10.1007/s13369-021-05533-7

16. Somatkar, A., Dwivedi, R., & Chinchanikar, S. (2024). Optimizing roller burnishing of aluminum alloy 6061-T6: Comparative analysis of dry and lubricated conditions for enhanced surface quality and mechanical properties. Journal of Manufacturing and Materials Processing, 9(11), 360. https://doi.org/10.3390/jmmp9110360

17. Sundar, L. S., Chandra Mouli, K. V. V., & Said, Z. (2024). Experimental measurement of thermal conductivity and viscosity of Al_2O_3–GO (80:20) hybrid and mono nanofluids: A new correlation. Materials Science and Engineering: B, 305, 117437. https://doi.org/10.1016/j.mseb.2024.117437

18. Tiwari, A., Agarwal, D., & Singh, A. (2021). Computational analysis of machining characteristics of surface using varying concentration of nanofluids (Al_2O_3, CuO and TiO_2) with MQL. Materials Today: Proceedings, 42(Part 2), 1262–1269. https://doi.org/10.1016/j.matpr.2020.12.950

19. Wakamatsu, T. (2024). Fatigue strength improvement of aluminum alloy with surface defect by ball burnishing. Fatigue & Fracture of Engineering Materials & Structures, 47(8), 2876–2890. https://doi.org/10.1111/ffe.14372

20. Yildırım, Ç. V., Sarıkaya, M., Kıvak, T., & Şirin, Ş. (2021). Tribology and machinability performance of hybrid Al_2O_3–MWCNTs nanofluids-assisted MQL for milling Ti-6Al-4V. International Journal of Advanced Manufacturing Technology, 117, 2007–2024. https://doi.org/10.1007/s00170-021-08279-6